RESEARCH ARTICLE

Inflammation and apoptosis accelerate progression to irreversible atrophy in denervated intrinsic muscles of the hand compared with biceps: proteomic analysis of a rat model of obstetric brachial plexus palsy

Xiao-Heng Yu[1, 2, #], **Ji-Xin Wu**[1, 2, #], **Liang Chen**[1, 2, *], **Yu-Dong Gu**[1, 2]

1 Department of Hand Surgery, Huashan Hospital and Institutes of Biomedical Sciences, Fudan University, Shanghai, China

2 Shanghai Key Laboratory of Peripheral Nerve and Microsurgery, Shanghai, China

Funding: *This work was supported by the National Natural Science Foundation of China, No. 816019591003263 (to JXW); the National Basic Research Program of China (973 Program), No. 2014CB542203 (to LC).*

Graphical Abstract

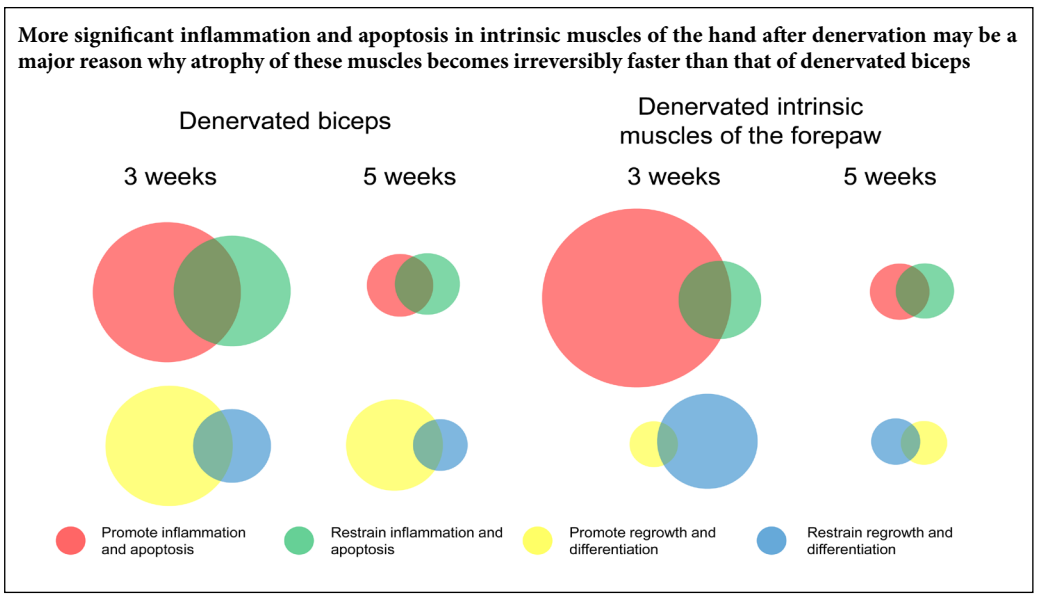

Correspondence to:
Liang Chen, MD, liangchen1960@163.com.

#Both authors contributed equally to this work.

orcid:
0000-0001-6585-8882 (Liang Chen)

doi: *10.4103/1673-5374.272619*

Received: *February 27, 2019*
Peer review started: *April 18, 2019*
Accepted: *June 27, 2019*
Published online: *January 9, 2020*

Abstract

In treating patients with obstetric brachial plexus palsy, we noticed that denervated intrinsic muscles of the hand become irreversibly atrophic at a faster than denervated biceps. In a rat model of obstetric brachial plexus palsy, denervated intrinsic musculature of the forepaw entered the irreversible atrophy far earlier than denervated biceps. In this study, isobaric tags for relative and absolute quantitation were examined in the intrinsic musculature of forepaw and biceps on denervated and normal sides at 3 and 5 weeks to identify dysregulated proteins. Enrichment of pathways mapped by those proteins was analyzed by Kyoto Encyclopedia of Genes and Genomes analysis. At 3 weeks, 119 dysregulated proteins in denervated intrinsic musculature of the forepaw were mapped to nine pathways for muscle regulation, while 67 dysregulated proteins were mapped to three such pathways at 5 weeks. At 3 weeks, 27 upregulated proteins were mapped to five pathways involving inflammation and apoptosis, while two upregulated proteins were mapped to one such pathway at 5 weeks. At 3 and 5 weeks, 53 proteins from pathways involving regrowth and differentiation were downregulated. At 3 weeks, 64 dysregulated proteins in denervated biceps were mapped to five pathways involving muscle regulation, while, five dysregulated proteins were mapped to three such pathways at 5 weeks. One protein mapped to inflammation and apoptotic pathways was upregulated from one pathway at 3 weeks, while three proteins were downregulated from two other pathways at 5 weeks. Four proteins mapped to regrowth and differentiation pathways were upregulated from three pathways at 3 weeks, while two proteins were downregulated in another pathway at 5 weeks. These results implicated inflammation and apoptosis as critical factors aggravating atrophy of denervated intrinsic muscles of the hand during obstetric brachial plexus palsy. All experimental procedures and protocols were approved by the Experimental Animal Ethics Committee of Fudan University, China (approval No. DF-325) in January 2015.

Key Words: *apoptosis; biceps; denervation; inflammation; intrinsic muscles of the hand; irreversible muscle atrophy; isobaric tags for relative and absolute quantitation; nerve regeneration; proteomic; rat models; reversible muscle atrophy*

Chinese Library Classification No. *R446; R363; R364*

Introduction

The consensus for treating infants with obstetric brachial plexus palsy is that nerve reconstruction surgery of the lower trunk should be performed up to 3 months postnatally (Chuang et al., 2005). For upper trunk injuries, the operation may be performed at 30 months or later (Boome et al., 2000). In a rat model of obstetric brachial plexus palsy, denervated intrinsic musculature of the forepaw (IMF) and denervated biceps had different histological features at different time points. We confirmed that it took a much shorter time for atrophy of denervated IMF to become irreversible compared with denervated biceps. This may be a key explanation for the more limited timing required for nerve reconstruction surgery of the lower trunk in obstetric brachial plexus palsy (Wu et al., 2013). In another study using a rat obstetric brachial plexus palsy model in which IMF atrophy was irreversible but that of the biceps remained reversible at 5 weeks after denervation, it was found that miRNA expression differed between the two denervated muscles. Moreover, Kyoto Encyclopedia of Genes and Genomes (KEGG) pathway analysis, as well as mapping of specifically dysregulated miRNAs and target genes, suggested that most affected pathways were involved in self-regulation of neuromuscular junctions (Pan et al., 2015). A further study emplying the same model showed that mRNA expression profiles in denervated IMF were lacking in genes mapping to pathways of muscular regrowth and differentiation compared with patterns in denervated biceps (Wu et al., 2016), indicating that insufficient levels of self-protective factors were one reason that the atrophic process of denervated IMF occurred more rapidly than in denervated biceps. However, these results provided little evidence for the involvement of inflammation and apoptosis in IMF, although these processes are considered to be critical for modulating atrophic processes in denervated muscles (Tidball et al., 2005).

After denervation, loss of muscle contraction leads to blood accumulation in the venous system, which induces leukocyte transmigration (Pober et al., 1990), aseptic inflammation (Iversen et al., 2005), and muscle cell apoptosis (Rowe et al., 2000). Theoretically, denervated IMF incurs more severe inflammation than denervated biceps because venous return is more hindered by gravity in the former. In our mRNA profiling study of the obstetric brachial plexus palsy model, only the p53 signaling pathway, which is associated with inflammation and muscle cell apoptosis, was upregulated in denervated IMF compared with the contralateral normal control (Wu et al., 2016). Based on reports that skeletal muscle inflammation occurred as early as 10 hours after nerve sectioning (Levine et al., 1990) and is preceded by onset of muscle cell proliferation (Murray et al., 1982), we believe that by sampling at 5 weeks after denervation, we missed peak expression of inflammation and apoptosis signaling in IMF. As atrophy becomes irreversible much sooner in denervated intrinsic muscles of the hand, we hypothesized that protein expression characteristics would differ between denervated IMF and biceps, with the former having more upregulated signaling related to inflammation and apoptosis than its contralateral counterpart. This study, therefore, aimed to test that hypothesis by dynamically analyzing protein expression profiles in denervated IMF and biceps.

Materials and Methods

Animal surgery and sample preparation

A total of 120 Sprague-Dawley rats were obtained at 7 days after birth from the Experimental Animal Science Department, Fudan University, China (license number: SYXK (Hu) 2014-0029). This study was approved by the Experimental Animal Ethics Committee of Fudan University, China (approval No. DF-325) in January 2015. After intraperitoneal injection of 10% chloral hydrate (300 mg/kg), each rat was placed in a supine position and the right brachial plexus was exposed through the supraclavicular route.

C5–C6 spinal nerves were lacerated and C7–C8–T1 were avulsed. After 3 weeks, 60 rats were sacrificed and samples of denervated IMF and biceps on the right side and their normal counterparts on the left side were harvested. Of these, samples from 40 rats were labeled with isobaric tags for relative and absolute quantitation (iTRAQ). Samples from the remaining 20 rats were analyzed by western blot assay to verify iTRAQ results. At 5 weeks after surgery, samples were obtained from the other 60 rats using the same procedures. To prepare samples for iTRAQ, muscles were frozen in liquid nitrogen and ground with a mortar and pestle. Next, buffer (4% sodium dodecyl sulfate and 0.1 M dithiothreitol in 0.1 M Tris-HCl, pH 7.6) was added to each sample and the resulting lysates were sonicated and boiled for 15 minutes. After centrifugation, protein levels were measured in supernatants with a bicinchoninic acid protein assay kit (Bio-Rad, Hercules, CA, USA). Protein solutions from denervated IMF were pooled, as were those from denervated biceps. Samples on the contralateral side were prepared using the same procedures. All mixtures of protein solutions were pre-processed by filter-aided sample preparation digestion. Protein suspensions were digested with 4 μg trypsin (Promega Biotech, Beijing, China) in 40 μL of dissolution buffer (SCIEX, Shanghai, China) overnight and the resulting peptides were collected as a filtrate. Peptides within each combined solution were desalted on C18 Cartridges (Empore™ SPE; Minnesota Mining and Manufacturing Company, St. Paul, MN, USA) and stored at –80°C.

iTRAQ labeling and LC-MS/MS analysis

iTRAQ was carried out at 3 and 5 weeks to examine prepared samples. According to the manufacturer's instructions (Applied Biosystems, Foster City, CA, USA), 100 μg of peptide mixture from each sample was labeled with iTRAQ reagents as follows: control IMF by 114 tag, denervated IMF by 115 tag, control biceps by 116 tag, and denervated biceps by 117 tag. Labeled peptides were fractionated by strong cation exchange chromatography using an AKTA Purifier system (GE Healthcare, Shanghai, China) and then desalted on C18 Cartridges. Samples were analyzed by liquid chromatography tandem mass spectrometry (LC-MS/MS). EASY-nLC™, a high-performance liquid chromatography system,

was used to separate each fraction, which was then analyzed on a Q-Exactive mass spectrometer (Thermo Fisher Scientific, Shanghai, China) in positive ion mode. The resolution of survey scans was set to 70,000 at 200 m/z, while that of high-energy collisional dissociation spectra scans was set to 17,500 at 200 m/z. Information-dependent acquisition was enabled with automatic collision energy.

Protein identification and quantitation

Protein identification was performed on each result of iTRAQ. LC-MS/MS spectra were searched using the MASCOT search engine (Matrix Science, UK; version 2.3) embedded into Proteome Discoverer 1.4 (Thermo Fisher Scientific, 2012). For protein identification, search parameters were as follows: maximum missed cleavages = 2, enzyme = trypsin, peptide mass tolerance = ± 20 ppm, and fragmented mass tolerance = 0.1 Da. Weighed and standardized quantitative protein ratios were determined between denervated IMF and control samples, and between denervated biceps and control samples. Only proteins with a fold change ≥ 1.5 and *P*-value < 0.05 were considered dysregulated. Differential expression of proteins was then depicted in volcano plots according to fold changes and *P*-values. Names of dysregulated proteins were designated using the format of UniProt Knowledgebase (https://www.uniprot.org).

Bioinformatics

KEGG database analysis (https://www.kegg.jp/) was applied to determine enriched pathways for dysregulated proteins identified in denervated IMF and biceps at 3 and 5 weeks. To identify the significance of pathways, either Fisher's exact or chi-square test was used to calculate *P*-values. Only KEGG pathways with *P*-values < 0.05 were considered significant.

Western blot assay

For IMF and biceps on both denervated and contralateral sides, 20 sets of samples were harvested at 3 weeks and 20 sets were collected at 5 weeks. Cytochrome c oxidase subunit 6C (COX6C) and myosin heavy chain 1 (MYH1) were randomly chosen for western blot assay to validate iTRAQ results. Radioimmunoprecipitation assay buffer was used to pre-process each tissue. Aliquots of 60 μg protein from each sample were separated by sodium dodecyl sulfate-polyacrylamide gel electrophoresis and transferred to membranes; glyceraldehyde-phosphate dehydrogenase (GAPDH) was used as the internal reference. Membranes were incubated with primary goat anti-rat polyclonal antibodies of COX6C or MYH1 respectively (1:1000; Goodbio Technology, Wuhan, China) overnight at 4°C and then with a horseradish peroxidase-conjugated donkey anti-goat secondary antibody (1:3000; Goodbio Technology) at room temperature for 30 minutes. An ECL detection system (Amersham Biosciences, Buckinghamshire, UK) was used to visualize stained bands, which were quantified by grayscale value ratios to the internal reference using AlphaEaseFC software (Alpha Innotech, San Leandro, CA, USA).

Statistical analysis

Data are expressed as ratios of grayscale values relative to internal controls. Statistical analysis was performed with SPSS 19.0 software (IBM, Armonk, NY, USA). A random variance model *t* test was used to test the distribution and identify dysregulated proteins by comparing protein expression in denervated muscles with their respective controls. For western blot assay, an independent two-tailed *t* test was used to compare results for each protein in denervated muscles with those in corresponding control muscles on the contralateral side. $P < 0.05$ was considered statistically significant.

Results

Proteomics and bioinformatics

iTRAQ results are shown in **Figure 1**. Compared with contralateral tissue, 845 dysregulated proteins were identified in denervated IMF at 3 weeks (**Figure 1A**), including 323 that were mapped to 60 pathways by KEGG analysis. Among KEGG database pathways related to muscle and nerve, 119 dysregulated proteins were mapped to nine pathways. Of those, five pathways with 27 upregulated proteins were related to inflammation and apoptosis, including cGMP-PKG, MAPK signaling, insulin, pyruvate metabolism, and HIF-1 pathways. The other four pathways, to which 98 downregulated proteins were mapped, were associated with regrowth and differentiation, including calcium signaling, tight junction, AMPK signaling, and fatty acid metabolism (**Table 1**). At 5 weeks, 448 dysregulated proteins were identified (**Figure 1C**), of which 225 were mapped to 20 pathways. There were 67 dysregulated proteins that mapped to three pathways connected to nerve and muscle, including: pyruvate metabolism with one upregulated protein related to apoptosis, calcium signaling with 25 downregulated proteins related to differentiation, and glycolysis/gluconeogenesis with 27 downregulated proteins associated with energy metabolism in muscle cells (**Table 1**).

Compared with the contralateral tissue, 592 dysregulated proteins were identified in denervated biceps at 3 weeks (**Figure 1B**), including 323 that were mapped to 35 KEGG pathways. Of these, 64 dysregulated proteins were mapped to five pathways related to muscle and nerve according to the KEGG database, including: pyruvate metabolism with one upregulated protein related to apoptosis; calcium signaling, fatty acid metabolism, and PPAR signaling with four upregulated proteins associated with regrowth and differentiation; and glycolysis/gluconeogenesis, which is related to muscle cell energy metabolism (**Table 2**). At 5 weeks, 44 dysregulated proteins were identified (**Figure 1D**), of which 32 were mapped to eight KEGG pathways. Five dysregulated proteins were mapped to three pathways related to muscle and nerve. Among these, taurine and hypotaurine metabolism, and pyruvate metabolism, which had three downregulated proteins, were related to apoptosis and fatty acid metabolism, while the other two downregulated proteins were associated with proliferation (**Table 2**).

Table 1 KEGG pathways, to which both upregulated and downregulated proteins in denervated IMF were mapped, at 3 and 5 weeks after denervation

Term	Count[a]	Protein name[b]	*P*-value
Pathways at 3 weeks			
cGMP-PKG pathway	21	F1LV12*, Q3HSE5*, P16067*, P63329, Q64578, P62142, P13638, B3XZL8, P07340, A0A0H2UHV6, G3V6V5, P06686, P61589, G3V731, P81155, Q9Z2L0, Q05962, D3ZB81, A0A0G2JSR0, P29117, Q64595	0.001
MAPK signaling	26	Q5BJU0*, D3Z8L7*, Q3HSE5*, Q62862*, G3V6P8*, B5DFH7*, Q6MGC8*, A0A0H2UHR7, D4AE17, P63329, P14659, P0DMW0, D3Z8E0, B1H230, G3V913, B3XZL8, Q925D6, A0A0H2UHV6, Q4G050, Q63538, Q6P727, A0A0G2K4U4, P53042, Q66H84, G3V6E5, F1LXV0	0.001
Insulin pathway	20	P12785*, A0A0G2K5G8*, Q3HSE5*, P12369*, G3V8R5*, Q9Z2S9*, P19357, M0RD75, D3ZM60, P13286, P27881, P62142, F1LLZ7, A2RRU1, P97531, G3V8V3, Q4G050, A0A0G2K9C8, Q6P727, Q9Z1N1	0.002
Pyruvate metabolism	17	A0A0G2K5G8*, P52873*, Q6P7Q4, P11980, P04636, A0A0G2K4C6, P35745, F7FKI5, P17764, O88989, P42123, P08461, P14408, Q6P6R2, A0A0G2JZH8, P49432, B0BN46	< 0.001
HIF-1 pathway	14	Q3HSE5*, Q9ET45*, P15429, M0RD75, A0A0G2K7M1, P27881, P07323, M0R660, Q4G050, F7FKI5, P49432, E9PTN6, P11275, G3V679, E9PTV9	0.006
Calcium pathway	22	F1LV12*, F1LMY4, P63329, Q304F3, Q64578, P13286, A0A0G2K5J1, F1LPJ2, Q4PP99, B3XZL8, F1LLZ7, A0A0H2UHV6, G3V731, P81155, A0A0G2K9C8, Q9Z2L0, Q05962, D3ZB81, A0A0G2JSR0, P29117, P11275, Q62711, F1LQL1	< 0.001
Tight junction	20	Q5BJU0*, A0A0G2JUX7*, D3Z8L7*, Q3HSE5*, D4AE17, P04466, A0A0G2JSQ0, A0A0G2K484, F1LRV9, D3ZCV0, P61589, G3V6E1, Q6GMN8, Q8K551, A0A0G2JYA4, Q29RW1, P62716, A0A0G2KA61, B1WC41, F1M4I1	0.003
AMPK signaling	16	P12785*, A0A0G2K5G8*, Q3HSE5*, G3V8R5*, P19357, A0A0G2JSQ0, Q52KS1, A2RRU1, Q5XIJ7, Q5PQN8, D4AC16, A0A0G2JYA4, Q9Z1N1, P62716, C9DRP4, Q63704	0.005
Fatty acid metabolism	12	P12785*, A0A0G2K5G8*, Q63151*, P33124, P17764, Q9WVK7, Q9WVK3, P08503, P70584, P14604, Q5M9H2, Q63704	0.002
Pathways at 5 weeks			
Glycolysis/ gluconeogenesis	29	G3V9W6*, P25113*, D3ZZN3, P07323, P30835, A0A0G2JZH8, Q6P9U7, E9PTN6, D4A5G8, Q9Z1N1, B1WBN9, P49432, E9PTV9, Q6P6R2, P08461, P27881, P09117, P16617, P42123, P48500, Q6P6G4, Q6P6V0, Q499Q4, M0R660, P16290, P15429, P11980, Q52KS1, P05065	< 0.001
Calcium signaling	29	G3V6Q6*, D3ZH00*, P15791*, Q09073*, P29117, P68182, D3ZB81, A0A0G2K5J1, P84903, A0A0G2JSR0, F1LMY4, Q4PP99, P13286, P81155, G3V9D1, G3V731, P11275, P20651, P63329, A0A0G2K9C8, A1L1M0, P10688, F1LLZ7, Q05962, Q9Z2L0, B3XZL8, F1LPJ2, Q304F3, Q64578	< 0.001
Pyruvate metabolism	20	G3V9W6*, D3ZJH9, D3ZZN3, A0A0G2K4C6, A0A0G2JZH8, Q6P9U7, D4A5G8, B1WBN9, P17764, P49432, P35745, Q6P6R2, P08461, B0BN46, P14408, P42123, O88989, Q6P7Q4, P04636, P11980	< 0.001

[a]Expression of proteins was compared between denervated IMF and normal IMF, the latter on the contralateral side. [a]This refers to the quantity of upregulated and downregulated proteins mapping to the pathway. [b]Protein name is shown in the format of the UniProt Knowledgebase. *Upregulated proteins in denervated IMF. No asterisk means downregulated proteins in denervated IMF.

Validation by western blot assay

Two proteins, cytochrome c oxidase subunit 6C (COX6C) and myosin heavy chain 1 (MYH1), were randomly selected from dysregulated proteins in denervated IMF and biceps for analysis by western blot assay to validate iTRAQ results. Based on densitometric values compared with the internal reference, MYH1 and COX6C were downregulated in both denervated IMF and denervated biceps compared with corresponding tissue on the contralateral side at 3 weeks ($P < 0.05$; **Figure 2A**). At 5 weeks, these two proteins were downregulated in denervated IMF, but upregulated in denervated biceps ($P < 0.05$; **Figure 2B**). These results were consistent with those obtained by iTRAQ.

Discussion

One of the primary reasons for failure of nerve repair is that muscle atrophy can become irreversible before regenerating nerves can reinnervate target muscles (Roganovic et al., 2005; Piras and Boido, 2018; Weng et al., 2018; Zhang et al., 2018). Using the obstetric brachial plexus palsy rat model, whereby atrophy of denervated IMF is irreversible but that of denervated biceps is reversible, our previous study showed that IMF and biceps had distinct miRNA expression patterns after denervation. In a subsequent study of mRNA profiles, pathways associated with muscular regrowth and differentiation were more active in denervated biceps than in denervated IMF. In the present study examining the same model at 3 weeks after denervation, nine pathways in IMF were identified by KEGG analysis and five of these were related to inflammation and apoptosis. The MAPK pathway, to which upregulated Ras-related protein and mitogen-activated protein kinase 5 were mapped in this study, reportedly recruited leukocytes and evoked inflammatory cascades during inflammation in denervated skeletal muscle (Li et al., 2005). HIF-1 signaling, for which BCL2/adenovirus E1B 19-kDa protein-interacting protein 3 was upregulated in this study, was previously shown to be activated during muscle injury (Taylor et al., 2008). The pyruvate metabolism pathway, to

Table 2 KEGG pathways, to which both upregulated and downregulated proteins in the denervated biceps were mapped, at 3 and 5 weeks after denervation

Term	Count[a]	Protein name[b]	*P*-value
Pathways at 3 weeks			
Glycolysis / Gluconeogenesis	22	P11884*, P07323, E9PTV9, P16617, P04642, P48500, P11980, P16290, P15429, Q52KS1, Q6P6V0, A0A0G2K7M1, E9PTN6, M0R660, Q9Z1N1, P05065, Q6P6R2, P08461, D3ZZN3, F7FKI5, P49432, A0A0G2JZH8	< 0.001
Pyruvate metabolism	17	P11884*, B0BN46, P04642, P11980, P35745, P14408, A0A0G2K4C6, Q6P6R2, P04636, P08461, D3ZZN3, F7FKI5, P49432, P17764, A0A0G2JZH8, A0A0G2K1W9, O88989	< 0.001
Fatty acid metabolism	18	O35547*, Q63151*, P70584, Q9WVK3, P33124, G3V9U2, P14604, P17764, P15651, Q64428, Q5M9H2, Q9WVK7, Q60587, P18163, P18886, P08503, P07896, G3V7N5	< 0.001
Calcium signaling	16	P11275, P20651, A0A0G2K9C8, P13286, Q64578, A0A0G2JSR0, F1LLZ7, Q304F3, G3V731, A0A0G2K5J1, F1LQL1, P29117, Q9Z2L0, Q05962, Q62711, D3ZB81	< 0.001
PPAR signaling	9	O35547*, Q63151*, P33124, M0R7S5, P18163, P18886, P08503, P07896, G3V7N5	0.008
Pathways at 5 weeks		F1LV12*, F1LMY4, P63329, Q304F3, Q64578, P13286, A0A0G2K5J1, F1LPJ2, Q4PP99, B3XZL8, F1LLZ7, A0A0H2UHV6, G3V731, P81155, A0A0G2K9C8, Q9Z2L0, Q05962, D3ZB81, A0A0G2JSR0, P29117, P11275, Q62711, F1LQL1	< 0.001
Taurine and hypotaurine metabolism	2	Q5PQV0*, A0A0G2K5P7	< 0.001
Fatty acid metabolism	2	A0A0G2K5G8, P12785	0.036
Pyruvate metabolism	2	A0A0G2K5G8, P13697	0.039

Expression of proteins was compared between the denervated biceps and the normal biceps, the latter on the contralateral side. [a]This refers to the number of upregulated and downregulated proteins mapping to the pathway. [b]Protein name is shown in the format of the UniProt Knowledgebase. *Upregulated proteins in the denervated biceps. No asterisk means downregulated proteins in the denervated biceps.

which downregulated pyruvate kinase and malate dehydrogenase were mapped, can inhibit apoptosis induced by free radicals (Kang et al., 2001). The cGMP-PKG pathway, to which downregulated cGMP-dependent protein kinase 2 was mapped, can reportedly mediate vasodilation and chemotaxis during inflammation (Browner et al., 2004). The insulin pathway, for which phosphorylase b kinase and 40S ribosomal protein were upregulated, was shown to inhibit migration of inflammatory cells into skeletal muscle (Wei et al., 2008). The remaining four activated pathways were related to regrowth and differentiation. Among these, the tight junction pathway (Röder et al., 2008), to which upregulated Ras-related protein and membrane-associated guanylate kinase were mapped in this study, and calcium signaling with downregulated calcium/calmodulin-dependent protein was mapped in a previous study (Wu et al., 2000), can enhance regeneration of muscle cells. In contrast, AMPK signaling (Motoshima et al., 2006) and the fatty acid metabolism pathway (Bonen et al., 1999), both with upregulated fatty acid synthase and cetyl-CoA carboxylase, can restrict regrowth of muscle cells. At 5 weeks, three pathways with dysregulated proteins were identified in denervated IMF: pyruvate metabolism with downregulated pyruvate kinase, calcium signaling with downregulated calcium/calmodulin-dependent protein, and glycolysis/gluconeogenesis with downregulated 6-phosphofructokinase, which can enhance energy metabolism in muscle cells (Kelley et al., 1988). These results suggest that in denervated IMF, peak inflammation and apoptosis occur earlier than 5 weeks after denervation, while signaling for regrowth and differentiation was stably expressed at low levels. As inflammation and apoptosis proceeded, the muscle structure was substantially damaged such that denervated IMF was deprived of its self-regulating ability, irreversibly becoming atrophic.

At 3 weeks in denervated biceps, upregulated and downregulated proteins were mapped to five pathways related to nerve and muscle including: pyruvate metabolism with downregulated pyruvate kinase, calcium signaling with downregulated adenylate cyclase type 2, fatty acid metabolism with upregulated fatty acid synthase and long chain fatty CoA ligase 2, glycolysis/gluconeogenesis with downregulated 6-phosphofructokinase, and PPAR signaling with upregulated long chain fatty acid CoA ligase 3. Notably, the PPAR signaling pathway can function in repair of denervated neuromuscular junctions (Da Cruz et al., 2012). At 5 weeks, five proteins that mapped to three pathways involving muscle and nerve were dysregulated. Of these, downregulated acetyl-CoA carboxylase was associated with pyruvate metabolism and upregulated gamma-glutamyltransferase 5 was related to taurine and hypotaurine metabolism, which can reportedly inhibit inflammation (Das et al., 2012). The third identified pathway, fatty acid metabolism, was the only pathway related to muscle cell regrowth and differentiation to which downregulated fatty acid synthase was mapped. In our previous study, mRNA microarray analysis of the same muscles at 5 weeks mapped upregulated mRNAs to five signaling pathways relevant to the promotion of muscle cell regrowth and differentiation (Wu et al., 2016). Possible reasons for identifying fewer pathways related to regrowth and differentiation at 5 weeks in this proteomic study include half-life differences (Maier et al., 2009) and variations in post-transla-

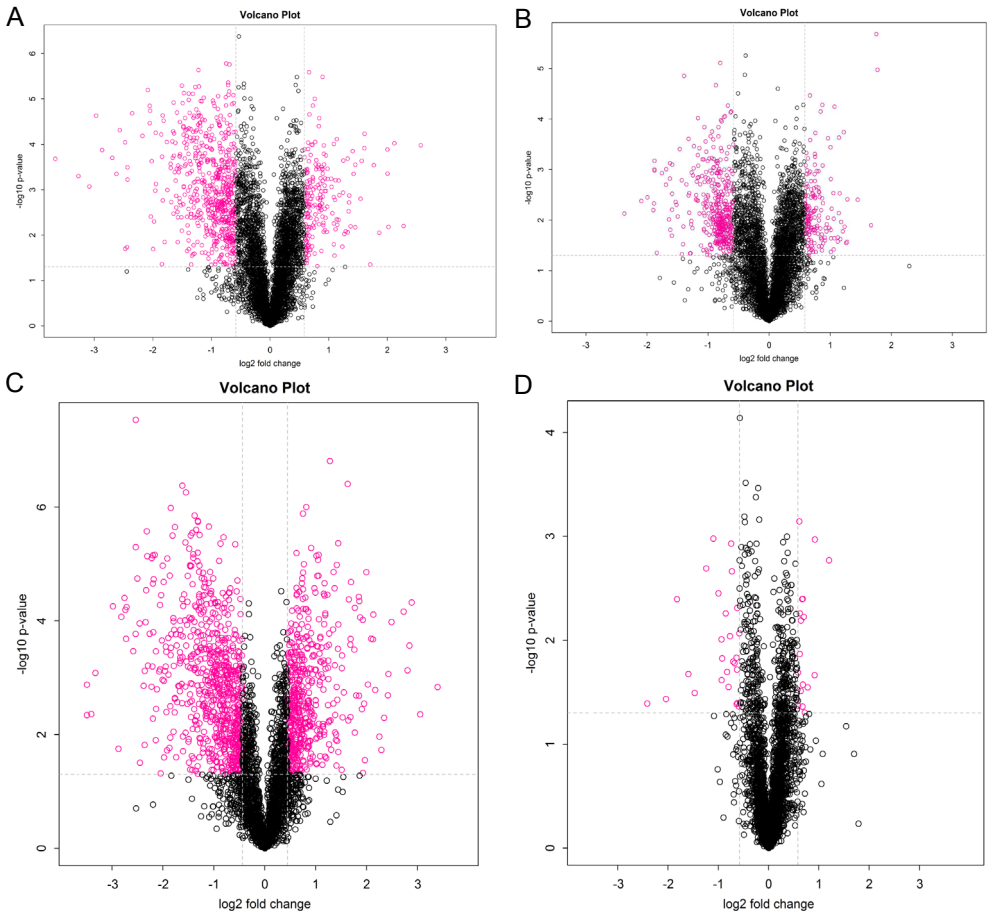

Figure 1 Volcano plots of protein expression ratios in denervated IMF and biceps at 3 and 5 weeks compared with respective contralateral controls.
(A–D) Volcano plots showing all proteins detected by iTRAQ in denervated IMF (A, C) and denervated biceps (B, D) at 3 (A, B) and 5 (C, D) weeks compared with corresponding muscles on the contralateral side. Pink dots represent proteins whose upregulation or downregulation was both statistically significant ($P < 0.05$) and 1.5-fold or more different from those in muscle on the contralateral side. Black dots indicate proteins whose dysregulation was either not statistically significant or had a statistical difference less than 1.5-fold relative to corresponding proteins on the contralateral side. IMF: Intrinsic musculature of the forepaw .

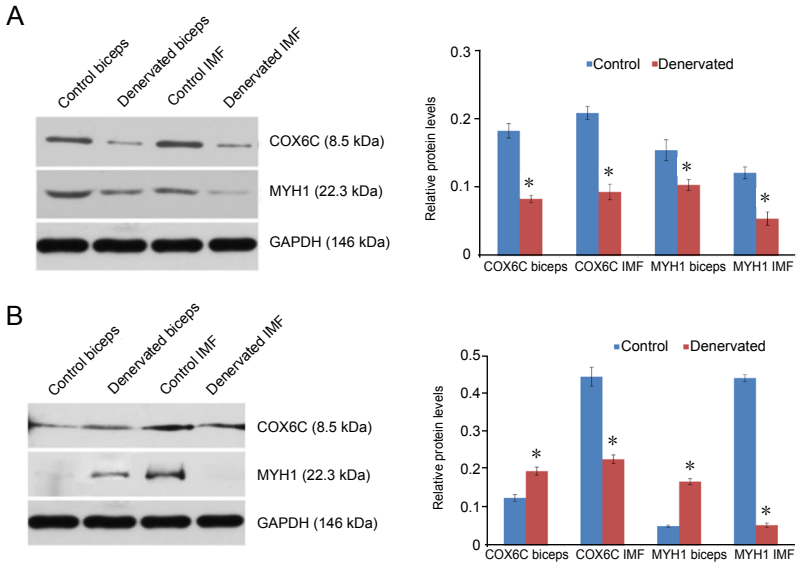

Figure 2 Validation of decreased MYH1 and COX6C protein levels at 3 and 5 weeks by western blot assay.
(A) Levels of MYH1 and COX6C proteins were decreased in denervated intrinsic musculature of the forepaw (IMF) and biceps compared with in biceps on the contralateral side at 3 weeks ($*P < 0.05$). (B) Levels of MYH1 and COX6C proteins were decreased in denervated IMF, but increased in the denervated biceps, compared with corresponding muscles on the contralateral side at 5 weeks ($*P < 0.05$). Representative western blot assay results are shown on the left, while ratios of grayscale values compared with the internal control are shown in the right. Verified proteins are indicated along the X-axis, while the Y-axis indicates the ratio of grayscale values between targeted protein and an internal reference. All results were consistent with data from iTRAQ.

tional modifications among identified proteins (Greenbaum et al., 2003). Regardless, our proteomic results comparing denervated biceps with its normal counterpart indicate that signaling for inflammation and apoptosis was inactive both at 3 and 5 weeks, suggesting that inflammation and apoptosis had not substantially damaged the structure of the denervated biceps at 5 weeks, such that its capacity for self-regulation was maintained and muscle atrophy remained reversible.

Denervation can lead to the onset of inflammation by stimulating neutrophil infiltration (Levine et al., 1990), and can also induce muscle apoptosis (Always et al., 2003). Our proteomic results suggest that after denervation, processes of inflammation and apoptosis in IMF were more intense than in biceps, at least at earlier time points. There are several potential reasons for this difference. First, coordinated and fine motor activities of the hand begin 10–12 months after birth (Schieber et al., 2004), while the embrace reflex, which is related to contraction of the biceps, appears prenatally

(Zafeiriou et al., 2004). This suggests that intrinsic muscles of the hand mature later than the biceps, leaving them more vulnerable to inflammation and apoptosis. Second, muscles controlling fine motor activities, such as facial and pharyngeal muscles, were clinically observed to be more susceptible to immune attack than limb muscles in myasthenia gravis (Evoli et al., 2003). Therefore, we speculated that intrinsic muscles in the hand, which manage complex and fine motor movements, are also more vulnerable than biceps to damage caused by denervation. Third, as intrinsic muscles of the hand are further from the heart than biceps, return of venous blood to the former is more hindered by gravity than flow to the latter. Indeed, because of greater venous congestion in denervated intrinsic muscles of the hand, the extent of inflammation may be more severe compared with denervated biceps. Based on the results of our proteomic analysis, which is just a macro analysis, we predicted potential causes underlying the different processes of irreversible muscle atrophy in intrinsic muscles of the hand and biceps. Therefore, more detailed experiments are needed to further validate the results.

In the rat model of obstetric brachial plexus palsy, whereby atrophy of IMF is irreversible but that of the biceps is reversible, our proteomic analysis suggested that pathways related to inflammation and apoptosis were clearly activated at 3 weeks, but significantly decreased at 5 weeks in denervated IMF; whereas, these pathways remained inactive both at 3 and 5 weeks in denervated biceps. This indicates that more significant inflammation and apoptosis in intrinsic muscles of the hand after denervation may be a major reason why atrophy of these muscles becomes irreversible faster than in denervated biceps.

Author contributions: *Study design: LC and YDG; fundraising: LC and JXW; experimental implementation and data analysis: XHY and JXW; paper writing: XHY. All authors approved the final version of the paper.*
Conflicts of interest: *The authors declare that there are no conflicts of interest associated with this manuscript.*
Financial support: *This work was supported by the National Natural Science Foundation of China, No. 816019591003263 (to JXW); the National Basic Research Program of China (973 Program), No. 2014CB542203 (to LC). The funding sources had no role in study conception and design, data analysis or interpretation, paper writing or deciding to submit this paper for publication.*
Institutional review board statement: *All experimental procedures and protocols were approved by the Experimental Animal Ethics Committee of Fudan University, China (approval No. DF-325) in January 2015. The experimental procedure followed the United States National Institutes of Health Guide for the Care and Use of Laboratory Animals (NIH Publication No. 85-23, revised 1996).*

Data sharing statement: *Datasets analyzed during the current study are available from the corresponding author on reasonable request.*
Plagiarism check: *Checked twice by iThenticate.*
Peer review: *Externally peer reviewed.*

Open peer reviewers: *Yuanyuan Liu, Boston Children's Hospital, USA; Ahmed Majeed Al-Shammari, Mustansiriyah University, Iraq.*

References

Always SE, Degens H, Krishnamurthy G, Chaudhrai, A (2003) Denervation stimulates apoptosis but not Id2 expression in hindlimb muscles of aged rats. J Gerontol A Biol Sci Med Sci 58:B687-697.
Bonen A, Dyck DJ, Ibrahimi, A, Abumrad NA (1999) Muscle contractile activity increases fatty acid metabolism and transport and FAT/CD36. Am J Physiol 276:E642-649.
Boome RS (2000) Traumatic branchial plexus injury. In: The growing hand: diagnosis and management of the upper extremity in children (Gupta A, Kay SPJ, Scheker LR, eds), pp 653-655. Mosby, London.
Browner NC, Sellak, H, Lincoln TM (2004) Downregulation of cGMP-dependent protein kinase expression by inflammatory cytokines in vascular smooth muscle cells. Am J Physiol Cell Physiol 287:C88-96.
Chuang DCC, Mardini S, Ma HS (2005) Surgical strategy for infant obstetrical brachial plexus palsy: experiences at Chang Gung Memorial Hospital. Plastic Reconstr Surg 116:132-144.
Da Cruz S, Parone PA, Lopes VS, Lillo C, McAlonis-Downes M, Lee SK, Williams DS (2012) Elevated PGC-1α activity sustains mitochondrial biogenesis and muscle function without extending survival in a mouse model of inherited. ALS Cell Metab 15:778-786.
Das J, Ghosh J, Manna P, Sil PC (2012) Taurine protects rat testes against doxorubicin-induced oxidative stress as well as p53, Fas and caspase 12-mediated apoptosis. Amino Acids 42:1839-1855.
Evoli A, Tonali PA, Padua L, Monaco ML, Scuderi F, Batocchi AP, Bartoccioni E (2003) Clinical correlates with anti-MuSK antibodies in generalized seronegative myasthenia gravis. Brain 126:2304-2311.
Greenbaum D, Colangelo C, Williams K, Gerstein M (2003) Comparing protein abundance and mRNA expression levels on a genomic scale. Genome Boil 4:117.
Iversen PO, Woldbaek PR, Christensen G (2005) Reduced immune responses to an aseptic inflammation in mice with congestive heart failure. Eur J Haematol 75:156-163.
Kang YH, Chung SJ, Kang IJ, Park JHY, Bunger R (2001) Intramitochondrial pyruvate attenuates hydrogen peroxide-induced apoptosis in bovine pulmonary artery endothelium. Mol Cell Biochem 216:37-46.
Kelley D, Mitrakou A, Marsh H, Schwenk F, Benn J, Sonnenberg G, Berger M (1988) Skeletal muscle glycolysis, oxidation, and storage of an oral glucose load. J Clin Invest 81:1563.
Levine JD, Coderre TJ, White DM, Finkbeiner WE, Basbaum AI (1990) Denervation-induced inflammation in the rat. Neurosci Lett 119:37-40.
Li YP, Chen Y, John J, Moylan J, Jin B, Mann DL, Reid MB (2005) TNF-α acts via p38 MAPK to stimulate expression of the ubiquitin ligase atrogin1/MAFbx in skeletal muscle. FASEB J 19:362-370.
Maier T, Güell M, Serrano L (2009) Correlation of mRNA and protein in complex biological samples. FEBS Lett 583:3966-3973.
Motoshima H, Goldstein BJ, Igata M, Araki E (2006) AMPK and cell proliferation–AMPK as a therapeutic target for atherosclerosis and cancer. J Physiol 574: 63-71.
Murray, MA, Robbins, N (1982) Cell proliferation in denervated muscle: time course, distribution and relation to disuse. Neuroscience 7:1817-1822.
Pan F, Chen L, Ding F, Zhang J, Gu YD (2015) Expression profiles of MiRNAs for intrinsic musculature of the forepaw and biceps in the rat model simulating irreversible muscular atrophy of obstetric brachial plexus palsy. Gene 565:268-274.
Piras A, Boido M (2018) Autophagy inhibition: a new therapeutic target in spinal muscular atrophy. Neural Regen Res 13:813-814.
Pober JS, Cotran RS (1990) The role of endothelial cells in inflammation. Transplantation 50:537-544.
Röder IV, Petersen Y, Choi KR, Witzemann V, Hammer III JA, Rudolf R (2008) Role of Myosin Va in the plasticity of the vertebrate neuromuscular junction in vivo. PLoS One 3:e3871.
Roganovic Z (2005) Missile-caused complete lesions of the peroneal nerve and peroneal division of the sciatic nerve: results of 157 repairs. Neurosurgery 57:1201-1212.
Rowe VL, Stevens SL, Reddick TT, Freeman MB, Donnell R, Carroll RC, Goldman MH (2000) Vascular smooth muscle cell apoptosis in aneurysmal, occlusive, and normal human aortas. J Vasc Surg 31:567-576.
Schieber MH, Santello M (2004) Hand function: peripheral and central constraints on performance. J Appl Physiol 96:2293-2300.
Taylor CT (2008) Interdependent roles for hypoxia inducible factor and nuclear factor-κB in hypoxic inflammation. J Physiol 586:4055-4059.
Tidball JG (2005) Inflammatory processes in muscle injury and repair. Am J Physiol Regul Integr Comp Physiol 288:R345-353.
Wei Y, Chen K, Whaley-Connell AT, Stump CS, Ibdah JA, Sowers JR (2008) Skeletal muscle insulin resistance: role of inflammatory cytokines and reactive oxygen species. Am J Physiol Regul Integr Comp Physiol 294:R673-680.
Weng J, Wang YH, Li M, Zhang DY, Jiang BG (2018) GSK3β inhibitor promotes myelination and mitigates muscle atrophy after peripheral nerve injury. Neural Regen Res 13:324-330.
Wu H, Naya FJ, McKinsey TA, Mercer B, Shelton JM, Chin ER, Simard AR, Michel RN, Bassel-Duby R, Olson EN, Williams RS (2000) MEF2 responds to multiple calcium-regulated signals in the control of skeletal muscle fiber type. EMBO J 19:1963-1973.
Wu JX, Chen L, Ding F, Gu YD (2013) A rat model study of atrophy of denervated musculature of the hand being faster than that of denervated muscles of the arm. J Muscle Res Cell Motil 34:15-22.
Wu JX, Chen L, Ding F, Chen LZ, Gu YD (2016) mRNA expression characteristics are different in irreversibly atrophic intrinsic muscles of the forepaw compared with reversibly atrophic biceps in a rat model of obstetric brachial plexus palsy (OBPP). J Muscle Res Cell Motil 37:17-25.
Zafeiriou DI (2004) Primitive reflexes and postural reactions in the neurodevelopmental examination. Pediatr Neurol 31:1-8.
Zhang C, Rong W, Zhang GH, Wang AH, Wu CZ, Huo XL (2018) Early electrical field stimulation prevents the loss of spinal cord anterior horn motoneurons and muscle atrophy following spinal cord injury. Neural Regen Res 13:869-876.

P-Reviewers: Liu Y, Al-Shammari AM; C-Editor: Zhao M; S-Editors: Wang J, Li CH; L-Editors: Deusen AV, Maxwell R, Qiu Y, Song LP; T-Editor: Jia Y